JOURNAL OF GEOPHYSICAL RESEARCH, VOL. 106, NO. D22, PAGES 28,189–28,197, NOVEMBER 27, 2001

Airglow observations of dynamical (wind shear-induced) instabilities over Adelaide, Australia, associated with atmospheric gravity waves

J. H. Hecht and R. L. Walterscheid

Space Science Applications Laboratory, The Aerospace Corporation, Los Angeles, California, USA

R. A. Vincent

Department of Physics and Mathematical Physics, University of Adelaide, Adelaide, South Australia, Australia

Abstract. While several observations have been made in recent years of instability features in airglow images of atmospheric gravity waves (AGWs), such measurements are still rare. To date, these features are characterized by appearing to be aligned perpendicular to the AGW wave fronts. Multi-instrument observations confirm the theoretical prediction that such features are caused by convective instabilities where the AGW-induced temperature variation causes the total lapse rate to exceed the adiabatic lapse rate. In February 2000, airglow observations were obtained at Buckland Park, Australia, which showed instability features with a different characteristic. These images showed small-scale (less than 10 km horizontal wavelength) features aligned parallel to the larger scale AGW wave fronts. These features were only seen in OH images, not in O2A images, indicating that they originate below 90 km altitude. Simultaneous MF radar wind data reveal the presence of a mean wind shear which, during the period of the small-scale features, was aligned nearly in the direction of AGW propagation. In addition, the larger scale AGW approached a critical level near 90 km altitude. While the wind shear itself is not large enough to cause an instability, an analysis of the data suggests that the small-scale features are the result of a dynamic (wind shear-induced) instability in the 87-90 km altitude region. The instability was due to a combination of the background wind shear and the large shear induced by the passage of the larger scale AGW as it approached the critical level.

1. Introduction

As atmospheric gravity waves (AGWs) propagate upward in altitude, eventually they dissipate by one of several mechanisms. The wind shears associated with the AGW may be great enough so that dynamical instabilities in the form of Kelvin-Helmholtz (KH) billows occur, the temperature gradients associated with the wave may be great enough so that a convective instability forms, or the wave may encounter a critical level where the wave velocity equals the wind velocity, and even in the absence of an instability, be absorbed into the mean flow through viscous dissipation. Although features suggesting KH billows have long been shown to exist in the mesosphere [e.g. *Lloyd et al.*, 1973], it is only recently, with the advent of advanced numerical models, lidars, radars, and airglow imagers, that more definitive studies have been possible.

Several recent studies have involved convective instabilities produced by breaking AGWs. *Fritts et al.* [1997] used a three-dimensional numerical simulation to show that when such instabilities occur they produce structures whose apparent phase fronts are aligned perpendicular to the phase fronts of the breaking AGW. They further showed that the existence of the convective instability, which occurs when the Richardson number (Ri) is less than 0 is not preempted by the formation of a dynamical instability when Ri is less than 0.25. In a series of papers, *Hecht et al.* [1997a, 2000] have observed these perpendicular structures at a time when lidar observations of the temperature gradient from 85 to 90 km have indicated the presence of a superadiabatic lapse rate. The observations have confirmed much of the *Fritts et al.* [1997] simulations. *Hecht et al.* [1997a] also argued that convective instabilities may be responsible for the ripple structures often seen in airglow images.

There has also been much investigation of the struc-

Paper number 2001JD000419.
0148-0227/01/2001JD000419$09.00

tures which form when dynamical instabilities occur [e.g., *Haurwitz*, 1964; *Lloyd et al.*, 1973; *Gossard and Hooke*, 1975; *Chandrasekhar*, 1981; *Fritts et al.*, 1996]. In the simplest situation of speed shear (no rotational shear), KH billow structures form whose apparent phase fronts are parallel to the phase fronts of the unstable AGW and perpendicular to the direction of the shear. *Lloyd et al.* [1973] actually observed KH billows which were aligned in the expected direction with respect to the unstable wind shear at an altitude just above 100 km. As these observations were made using a chemical release from a sounding rocket, this was only a snapshot of the event. A definitive observation of the relationship of an AGW to the instabilities could not be made. *Taylor and Hapgood* [1990] have argued that the ripples seen in airglow images are mainly due to such instabilities and thus KH billows could be common near the mesopause. *Larsen* [2000a, 2000b] has recently argued that large persistent winds with large often unstable wind shears are a common feature of the altitude region above 80 km, and thus dynamical instabilities are not unusual. These studies argue that the frequently observed quasiperiodic radar echoes and the associated sporadic E are due to these instabilities. However, observations which show AGWs breaking down and forming these parallel structures appear to be rare.

The importance of critical layers in the dynamics of the atmosphere has long been recognized [e.g., *Bretherton*, 1966; *Booker and Bretherton*, 1967; *Hines*, 1968; *Breeding*, 1971; *Gossard and Hooke*, 1975; *Huang et al.*, 1998; *Gardner and Taylor*, 1998]. In the simplest case, as the AGW approaches a critical layer, the vertical wavelength decreases and the wave dissipates via viscous dissipation and accelerates the mean flow. This has apparently been observed [*Huang et al.*, 1998]. However, *Gossard and Hooke* [1975] summarize a number of other possibilities such as the wave becoming dynamically unstable and breaking down. Because of the few observations, the fate of a wave as it approaches a critical level is still unclear.

This study reports on an unusual observation of an AGW in the presence of a background wind shear which is not by itself unstable. As a critical layer is encountered the wave forms features which are consistent with the presence of KH billows. These results allow a unique observational characterization of a KH instability arising from a combination of background shears and wave-induced wind shears associated with a critical level interaction near the mesopause.

2. Experimental Instrumentation

The observations reported on in this paper were obtained between 0100 and 0400 local time (LT) on February 16, 2000, at the Buckland Park Field Station located approximately 40 km north of Adelaide, Australia (35^0S, 138^0E). Data from two instruments at the field station were used in this analysis.

One instrument is a modified version of the Aerospace CCD nightglow camera which was originally described by *Hecht et al.* [1994]. This instrument obtains images of the OH Meinel (hereinafter OHM) and O2 Atmospheric (hereinafter O2A) band emissions. A sequence of five images are obtained, each at 1 min integration, through separate narrow passband filters. Two of the filters cover two different rotational lines of OH meinel (6,2) band, two filters cover different portions of the O2 Atmospheric (0,1) band, and one filter covers the background and has almost no airglow emission in its passband. The latter is used to correct the airglow images for background skylight. Thus one can obtain, besides images of the airglow, the intensity and temperature of the OH Meinel and O2 Atmospheric emissions. Examples of this technique are found in previous studies [*Hecht et al.*, 1997a, 1997b; *Hecht et al.*, 2000].

For this work the imager has been upgraded and now uses a 1536 by 1024 Kodak CCD chip. The pixels are binned 8 x 8 resulting in images that have 192 x 128 pixels. The resultant field of view is now 46° by 69° giving a field of view at 90 km altitude of approximately 75 x 122 km.

Wind measurements are obtained from the Buckland Park Medium Frequency (MF) radar operated in the spaced antenna mode. The wind measurements are reported every 2 km, although they represent an average over 4 km centered at that altitude. The data are also averaged over 20 min. Since the existence of data depends on the presence of suitable scattering irregularities, there are some periods (notably at 86 km at 0220 local time) where data were not recorded. In those cases data are interpolated between higher and lower altitudes.

3. Observations

The results of the observations are given in the following figures. Figure 1 shows OHM image data for six periods between 0229 and 0306 LT. The first panel at 0229 LT shows a brightening feature in the upper right (NW) corner. This bright feature moves toward the lower left (SE) portion of the image in subsequent images. This brightening is caused by an atmospheric gravity wave that is perturbing the OHM airglow, as has been seen frequently in airglow imagers [e.g., *Taylor and Hapgood*, 1990; *Hecht et al.*, 1997a, 1997b]. The direction of the AGW motion is shown as a white line. The most notable feature of this set of images, however, is the fine structure which first appears at 0236 LT and appears to propagate with the wave in subsequent images. The alignment of these structures is shown as a black line in the last image. Note that when another wavefront appears at 0259 LT the fine-scale structure does not appear. Corresponding images of the O2A show evidence for the larger scale wave but not for the fine structure.

Figure 2 shows the intensity along the white line for

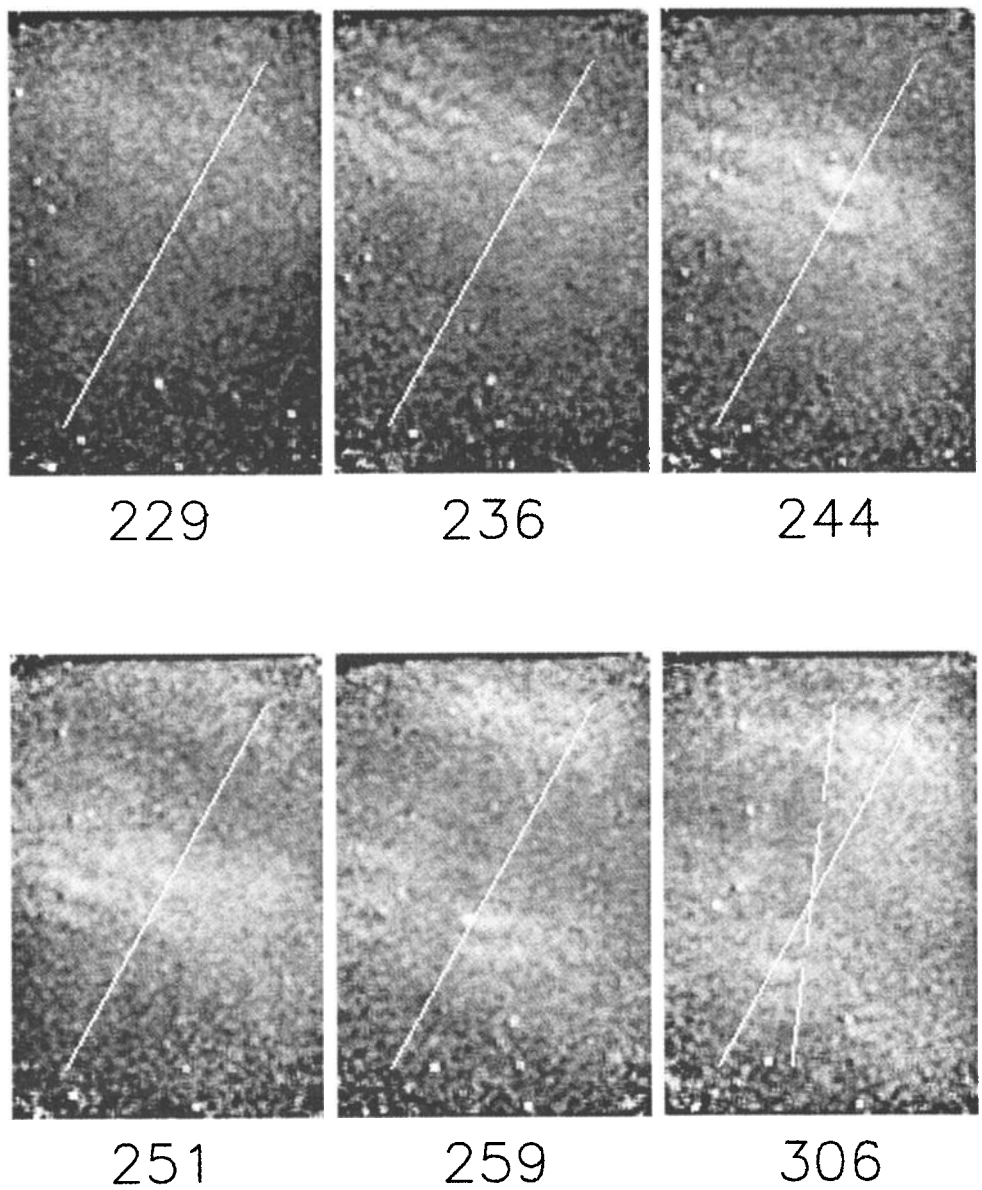

Figure 1. Six Images of the OH airglow obtained on February 16, 2000, local time from Buckland Park Observatory, north of Adelaide, using the Aerospace airglow camera. For each image, north is at the top and west is to the right. Each image has 128 x 192 pixels with each pixel being about 0.6 km at a nominal 90 km altitude. The field of view is about 46° by 69°. The six images were taken at 0229, 0236, 0244, 0251, 0259, and 0306 local time. Each image was exposed for 1 min through a 843.0 nm narrowband filter which covers one rotational line from the OH (6,2) band. A separate image through a non-OH filter was subtracted from each image. The images are scaled so that the brightest OH emission appears as white. The diagonal white line shows the direction of the AGW which is seen to propagate through the images. The dashed line at 0306 shows the approximate direction of the instability features.

the six images. These data allow an estimate of several features of the AGW and its instability. The horizontal wavelength of the AGW is $\approx 48 \pm 5$ km and its velocity with respect to the ground is $\approx 27 \pm 3$ m s^{-1}. The separation of the fine-scale features is between 7 and 9 km. The features appear at the peak of the presumed parent AGW and appear to be moving with the same velocity as the AGW. The magnitude of the AGW fluctuation is about 20% with respect to the background. The magnitude of the fine-scale features reaches about 10%.

Figure 3 shows the OHM and O2A intensities and temperatures before, during, and after the observation period. A large-scale wave with a period of about 3 hours is obvious in the OHM intensity data. It is not obvious in the O2A data. However, the most notable feature of these plots is that during the period of instability the OHM and O2A temperatures are nearly

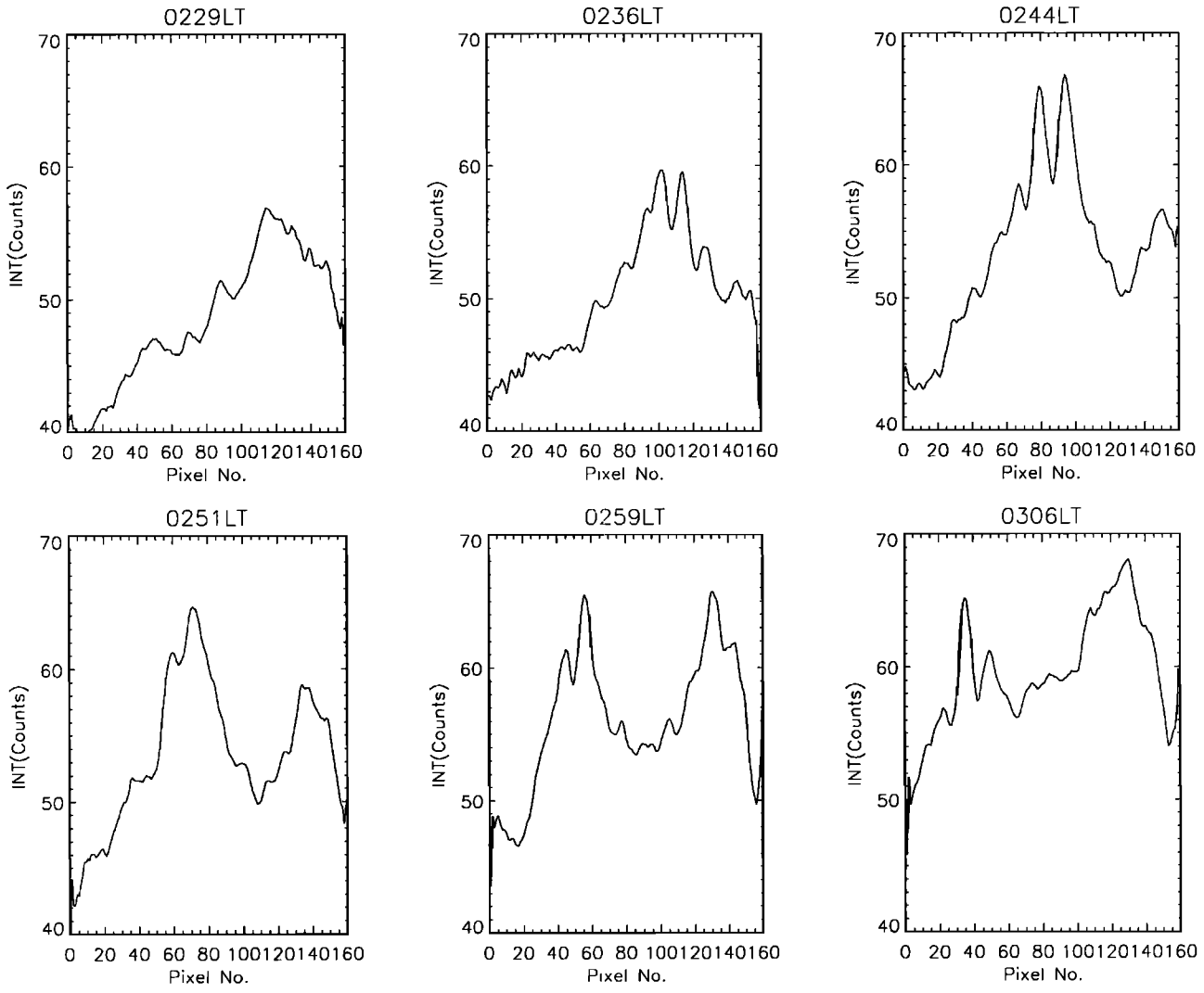

Figure 2. Six plots of the OH intensity as a function of pixel number along the white lines shown in Figure 1. Each pixel represents ≈ 0.6 km.

equal to each other with OHM temperatures actually lower than O2A temperatures. This suggests a stable atmosphere with respect to convective instabilities and is in direct contrast with what was found during observations of convective instabilities [*Hecht et al.*, 2000].

The existence of a dynamical instability then depends on the wind profile. Figure 4 shows four hodographs of the wind. In these plots east is to the right and north is to the top so as to correspond to the directions in the images shown in Figure 1. The upper left covers the period from 0200 to 0220 LT and each successive plot is 20 min later than the one preceding. The dashed line in each plot shows the magnitude and direction of the parent wave. At 0200 the winds below 92 km are less than the AGW phase velocity, indicating that there is no critical layer interaction at those altitudes. There appears to be the beginning of a shear in the direction of wave propagation between 86 and 88 km. However, the magnitude of the shear is small (below 20 m $s^{-1}km^{-1}$) and below the nominal 40 m $s^{-1}km^{-1}$ needed for Ri to be less than 0.25 for standard temperature profiles at these altitudes. At 0220 LT the shear is directly along the wave propagation vector, although its magnitude is still small. At 90 km the wind velocity just exceeds the AGW velocity. Since the OHM emission typically peaks near 90 km [*Hecht et al.*, 1997a], this suggests that the AGW may be encountering a critical layer. At 0240 LT the wind velocities exceed the AGW phase velocity at altitudes below 88 km. The magnitude of the shear has increased, but the direction is somewhat rotated from the direction of the AGW. At 0300 LT the winds between 88 and 90 km continue to increase.

Finally, Figure 5 shows the time history of the winds at 88 and 90 km from 0100 to 0420 LT. The winds at these altitudes appear to show the existence of a large-scale wave whose period is near 6 hours. The top panel shows the winds at 88 km. Between 0220 and 0300 there is an acceleration of the winds in the direction of the wave velocity with the winds exceeding the wave velocity after 0240 LT. The shear between 86 and 88 km increases from 15 to about 30 m $s^{-1}km^{-1}$ between 0220 and 0300 LT. At 90 km, as shown in the bottom

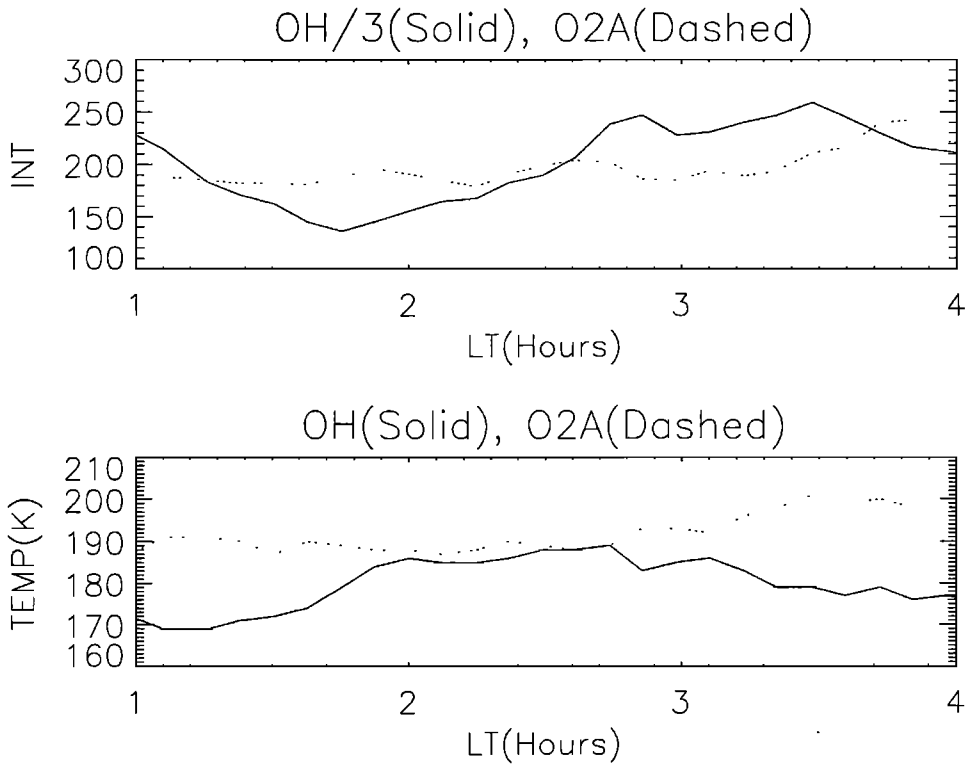

Figure 3. (top) Plots of the intensity, in rayleighs, as a function of local time for OHM (solid) and O2A (dashed). The OHM intensities have been reduced by a factor of 3 for clarity. (bottom) Same as top but for temperature. The OHM data have not been scaled.

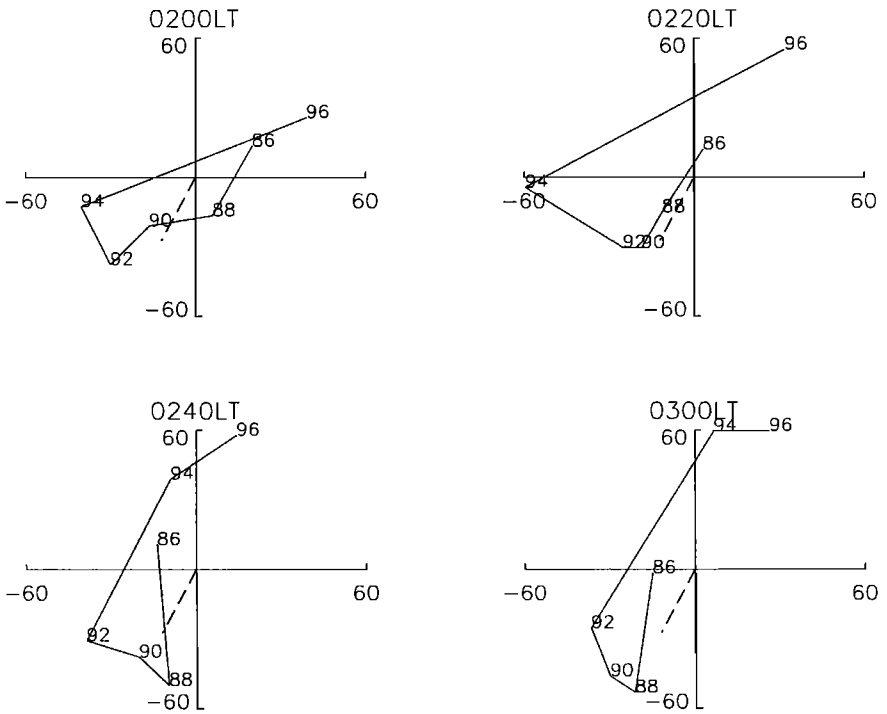

Figure 4. Four hodographs of the winds, averaged over time and altitude, obtained from the MF radar. The altitudes shown in each graph are every 2 km from 86 to 96 km. The winds at each altitude are averaged over a 4 km vertical extent centered at that altitude. The times are the start time of each 20 min average. For consistency with Figure 1 the winds are shown as positive north and west. The dashed line in each plot is the direction and magnitude, in m s^{-1}, of the AGW velocity along the white line in Figure 1.

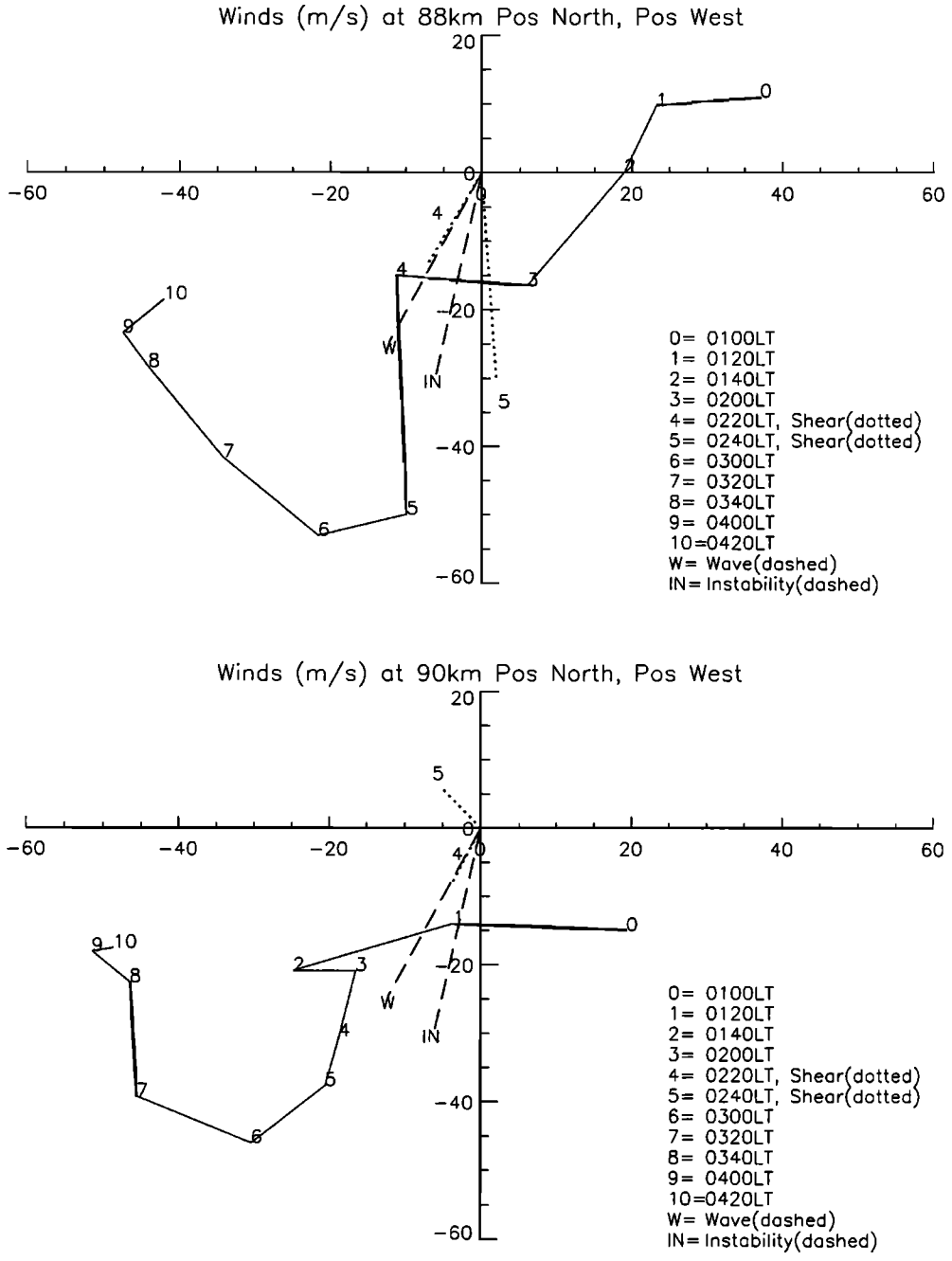

Figure 5. Two hodographs of the wind at two different altitudes as a function of time from 0100 to 0420 local time: (top) for 88 km and (bottom) for 90 km. Also shown in each plot as dashed lines are the direction and magnitude, in m s^{-1}, of the AGW from Figure 1 and the direction of the instability shown as a dashed line in the last image in Figure 1. The directions of the shear between the designated height and 2 km lower for two different times are shown as dashed lines. The magnitude of the shear is in m $s^{-1}km^{-1}$.

panel, the winds exceed the AGW velocity after 0220 LT. Only around 0220 to 0240 LT, however, is the shear in the direction of the AGW.

4. Discussion

The above results show the existence of an apparent instability feature which forms around 0240 LT. Given that the structures are aligned parallel to the crest of the main wav, and that there does not appear to be a large temperature gradient between OHM and O2A which nominally peak near 87 and 94 km, respectively, it is presumed that the structures are not due to a convective instability.

However, given that the structures are aligned along the direction of the wave and perpendicular to the background wind shear, it is possible that they are due to a dynamical (wind shear) instability, i.e., they are Kelvin Helmholtz billows. For this to be possible however, Ri must be below 0.25. Ri is given by

$$Ri = \frac{(g/T)(dT/dz + g/C_p)}{(dU/dz)^2} \quad (1)$$

where g is the acceleration of gravity, T is the atmospheric temperature, g/C_p is the adiabatic lapse rate which is about 9.5 K km^{-1}, dU/dz is the vertical wind shear, and z is altitude. Thus the numerator is the square of the Brunt-Vaisala frequency. For a temperature of 190 K, a nominal temperature lapse rate of 2 K km^{-1}, and a shear of 20 m s^{-1}km^{-1}, Ri is well above 0.25. For this temperature a wind shear of about 40 m s^{-1}km^{-1} is required for Ri to be below 0.25.

During the period when the structures appear, the wind velocity exceeds the AGW phase velocity at 90 km and is only slightly above the wave velocity at 88 km. Thus the intrinsic phase velocity and hence the vertical wavelength are decreasing with altitude. Following the equations given by *Hecht et al.* [1997a], the vertical wavelength for the presumed parent AGW is about 8 km at altitudes where the background wind is zero. However, this would reduce to about 2 km when the intrinsic phase velocity is reduced to around 5 m s^{-1}. Thus just around the time when the structures appear the AGW vertical wavelength is quite small at altitudes around 88 km. This means that the wind shear (and temperature gradient) induced by the AGW can be large.

The resultant value for Ri due to such a wave-induced wind shear is calculated as follows. An intensity perturbation of the AGW parent of about 20% peak to peak implies a temperature perturbation of about 4% peak to peak following *Schubert et al.* [1991], who give expressions relating intensity and temperature perturbations. This would result in the amplitude of the temperature wave being 2% or about a 4 K perturbation. Following *Hecht et al.* [1997a], an estimate can be made of the wind perturbation associated with this temperature perturbation. It is around 10 m s^{-1}. Using these numbers, and noting that the temperature and winds are 90° out-of-phase, Ri was calculated assuming a background wind shear of 20 m s^{-1}km^{-1} and a wave-induced shear consistent with vertical wavelengths from 0.5 to 3 km. The maximum extent of the region where Ri was less than 0.25, and thus implying an unstable region, occurred for vertical wavelengths around 2 to 2.5 km. (For vertical wavelengths below 1.5 km the unstable region is thinner, and for vertical wavelengths above 2.5 km the wave-induced shear is too small to cause an unstable region.) For the 2 to 2.5 km vertical wavelength AGWs the unstable region occupied about 1 km vertical extent.

For nominal atmospheric kinematic viscosity of $\approx$ 300 m^{2}s^{-1} [*Gardner and Taylor*, 1998] those Doppler-shifted waves with vertical wavelengths below about 3 km become subject to viscous dissipation [see *Gossard and Hooke*, 1975]. Based on *Gossard and Hooke* [1975] and *Hines* [1960], a time-scale t_d for the energy dissipation of the wave due to viscosity is given by $\approx 2/(Dm^2)$ where D is the kinematic viscosity and m is the vertical wave number given by $2\pi/\lambda$, where λ is the vertical wavelength. Thus when λ is 3 km t_d is $\approx$ 25 min, and when λ is 2 km t_d is $\approx$ 11 min. For a 1 km wave, t_d is even lower, about 3 min. *Larsen* [2000b] and *Fritts et al.* [1996] discuss the timescale for the evolution of KH billows from an instability. This timescale is given by $\approx 22(H/c)$ where H is the atmospheric scale height, taken to be near 6 km, and c is the speed of sound, taken to be near 300 m s^{-1}. With these values this timescale is approximately 7 min. Thus for waves with vertical wavelengths much below 2 km viscous dissipation will damp the wave before an instability develops.

Following *Lloyd et al.* [1973] and *Larsen* [2000b], it is estimated that the spacing of the structures is about 8 times the depth of the unstable region or about 8 km, consistent with the observations. These structures (KH billows) should have a thickness of 4 to 5 km. After the structures form they propagate with a velocity equal to the mean wind in the unstable region. Since the maximum in the wind shear induced by the AGW occurs where the velocity of the wave-induced perturbation is zero, the velocity of the structures depends on the background wind profile. This is not well known since the radar observations are averages over a few kilometers. Note, however, that the wind velocity near the altitude of the instability region (88 km) is increasing at later times to values close to or slightly above the AGW phase velocity. Thus it might be expected that the structures should be carried along with approximately the AGW velocity.

At slightly higher altitudes, however, above the altitude where we calculate the instability occurs, the vertical wavelength of the wave becomes less than 2 km, as the wind velocity nearly equals the wave velocity. Based on the dissipation timescales estimated above, the vertical wavelength is small enough so that rapid and significant viscous dissipation should occur somewhat before a critical level is encountered. Thus it would be expected that above the instability region the momentum transferred by the wave is transferred to the mean flow and the background wind velocities should increase, as is observed.

The above model can also be used to calculate the possibility of a convective instability. The results of such an analysis for a 2 or 2.5 km vertical wavelength wave are that there is a 0.5 to 1 km altitude region where the total temperature gradient is less than -9.5 K km^{-1}. (For the other modeled waves the vertical extent of this large negative temperature gradient is even smaller.) *Fritts et al.* [1997] argue that for a convective instability the spacing of the instability features should be about twice the depth of the unstable region. The data presented by *Hecht et al.* [1997a] suggest this ratio could be as high as a factor of 3. Either way for the present case this would imply a spacing of 1 to 3 km which is much less than the 7 to 9 km we observe. Note that for a convective instability, the spacing of 7 to 9

km implies a 2 to 4 km unstable region and a consequent large 20 K to 40 K decrease in temperature. The OHM and O2A airglow temperatures are nearly equal, suggesting almost no temperature gradient consistent with the small 2K km^{-1} background assumed in the dynamical instability model calculation.

The implications of these results are potentially significant as they show that AGW critical layer interaction can increase the background wind and thereby increase the background shear. Thus this mechanism may be part of what is causing the very large, and to date unexplained, winds and shears reported on by *Larsen* [2000a, 2000b].

5. Conclusions

The results of this study are as follows.

1. Images of the OHM airglow show the presence of an approximate 48 ± 5 km horizontal wavelength wave traveling at ≈ 27 ± 3 m s^{-1} between about 0200 and 0300 LT. The emission fluctuation has a peak to peak perturbation of about 20% of the background airglow. Around 0240 LT, fine-scale structure, whose separation is between 7 and 9 km, appears at the crest of the wave. The phase fronts of the fine-scale features appear to be parallel with the phase front of the parent AGW.

2. Measurements of the OHM and O2A temperature indicates little evidence for any unstable large-scale temperature gradient. This combined with the alignment of the structure parallel to the AGW phase front argues against a convective instability.

3. The wind data show wind velocities in the direction of the AGW exceeding the wave velocity at altitudes above 90 km around 0220 LT and exceeding the wave velocity at altitudes above 88 km 20 min later. This suggests a critical layer gravity wave interaction at altitudes just below 90 km. After 0220 LT the winds at altitudes around 88 to 90 km appear to accelerate in the direction of the wave.

4. A background wind shear whose magnitude is between 15 and 30 m $s^{-1}km^{-1}$ is observed oriented in the direction of the AGW from 0220 to 0300 LT. This shear by itself is not great enough to cause a dynamical instability to form. That requires about 40 m $s^{-1}km^{-1}$.

5. Consistent with the above results, it is proposed that as the wave velocity approaches the wind velocity below 88 km, the vertical wavelength of the AGW decreases, resulting in an increased total wind shear due to the superposed AGW induced and background shear. The total shear then becomes large enough to become dynamically unstable and form Kelvin-Helmholtz billows. This is the proposed cause for the origin of the fine-scale structure.

6. Based on the magnitude of the AGW perturbation, it is estimated that the temperature perturbation induced by the wave is about 4 K and the wind perturbation is about 10 m s^{-1}. Using these numbers, a calculation was made of the vertical extent of the region where Ri is less than 0.25 as the vertical wavelength decreases to values below 3 km. It was found that the vertical extent of the region is about 1 km for vertical wavelengths from 1.5 to 3 km.

7. For a 1 km thick unstable region the spacing of the fine-scale structure should be about 8 km, consistent with the observations. The Kelvin-Helmholtz billows should have a vertical height of 4 to 5 km, which if they are originating below 88 km would be consistent with observations in the OHM images but not in the O2A images.

8. The acceleration of the wind in the direction of the AGW suggests that some of the momentum transferred by the wave is being transferred into the mean flow.

Acknowledgments. We wish to thank the staff of the Buckland Park Observatory and especially Jonathon Woithe for support given in maintaining the Aerospace instrument. The Aerospace work was supported in part by NSF grant ATM-9813834 and by Aerospace Independent Research and Development funding.

References

Booker, J. R., and F. P. Bretherton, The critical layer for internal gravity waves in a shear flow, *J. Fluid Mech.*, *27*, 513-539, 1967.

Breeding, R. J., A non-linear investigation of critical levels for internal atmospheric gravity waves, *J. Fluid Mech.*, *50*, 545-563, 1971.

Bretherton, F. P., The propagation of groups of internal gravity waves in a shear flow, *Quart. J. Roy. Meteorol. Soc.*, *92*, 466-480, 1966.

Chandrasekhar, S., *Hydrodynamic and Hydrodynamic Stability*, 652 pp., Dover, Mineola N. Y., 1981.

Fritts, D. C., T. L. Palmer, O. Andreassen, and L. Lie, Evolution and breakdown of Kelvin-Helmholtz billows in stratified compressible flows. 1, Comparison of two- and three-dimensional flows, *J. Atmos. Sci.*, *53*, 3173-3191, 1996.

Fritts, D. C., J. R. Isler, J. H. Hecht, R. L. Walterscheid, and Ø. Andreassen, Wave breaking signatures in sodium densities and OH nightglow, 2, Simulation of wave and instability structures, *J. Geophys. Res.*, *102*, 6669-6684, 1997a.

Gardner, C. S., and M. J. Taylor, Observational limits for lidar, radar, and airglow imager measurements of gravity wave parameters, *J. Geophys. Res.*, *103*, 6427-6437, 1998.

Gossard, E. E., and W. H. Hooke, *Waves in the Atmosphere, Atmospheric Infrasound and Gravity Waves: Their Generation and Propagation*, 456 pp., Elsevier Sci., New York, 1975.

Haurwitz, B., Comments on wave forms in noctilucent clouds, *Geophys. Inst. Sci. Rep. No. UGAR 160*, Univ. of Alaska, Fairbanks, Alaska 1964.

Hecht, J. H., R. L. Walterscheid, and M. N. Ross, First measurements of the two-dimensional horizontal wavenumber spectrum from CCD images of the nightglow, *J. Geophys. Res.*, *99*, 11,449-11,460, 1994.

Hecht, J. H., R. L. Walterscheid, D. C. Fritts, J. R. Isler, D. C. Senft, C. S. Gardner, and S. J. Franke, Wave breaking signatures in OH airglow and sodium densities and temperature, 1, Airglow imaging, Na lidar, and MF radar observations, *J. Geophys. Res.*, *102*, 6655-6668, 1997a.

Hecht, J. H., R. L. Walterscheid, J. Woithe, L. Campbell, R. A. Vincent, and I. M. Reid, Trends of airglow imager ob-

servations near Adelaide, Australia, *Geophys. Res. Lett., 24*, 587-590, 1997b.

Hecht, J. H., C. Fricke-Begemann, R. L. Walterscheid, and J. Höffner, Observations of the breakdown of an atmospheric gravity wave near the cold summer mesopause at 54°N, *Geophys. Res. Lett., 27*, 879-882, 2000.

Hines, C. O., Internal atmospheric gravity waves at ionospheric heights, *Can. J. Phys.*, 55, 441-445, 1960.

Hines, C. O., Some consequences of gravity-wave critical layers in the upper atmosphere, *J. Atmos. Terr. Phys., 30*, 837-843, 1968.

Huang, T. Y., H. Hur, T. F. Tuan, X. Li, E. M. Dewan, and R. H. Picard, Sudden narrow temperature-inversion-layer formation in ALOHA-93 as a critical-layer-interaction phenomenon, *J. Geophys. Res., 103*, 6323-6332, 1998.

Larsen, M. F., Coqui 2: Mesospheric and lower thermospheric wind observations over Puerto Rico, *Geophys. Res. Lett., 27*, 445-448, 2000a.

Larsen, M. F., A shear instability seeding mechanism for quasi-periodic radar echoes *J. Geophys. Res., 105*, 24,931-24,940, 2000b.

Lloyd, K. H., C. H. Low, and R. A. Vincent, Turbulence, billows, and gravity waves in a high shear region of the upper atmosphere, *Planet. Space Sci., 21*, 653-661, 1973.

Schubert, G., M. P. Hickey, and R. L. Walterscheid, Gravity wave-driven fluctuations in OH nightglow from an extended dissipative emission region, *J. Geophys. Res., 96*, 13,869-13,880, 1991.

Taylor, M. J., and M. A. Hapgood, On the origin of ripple-type wave structure in the OH airglow emission, *Planet. Space Sci., 38*, 1421-1430, 1990.

J. H. Hecht and R. L. Walterscheid, Space Science Applications Laboratory, The Aerospace Corporation, M2-259, P. O. Box 92957, Los Angeles CA 90009, USA. (james.hecht@aero.org; richard.walterscheid@aero.org)

R. A. Vincent, Department of Physics and Mathematical Physics, University of Adelaide, Adelaide, South Australia, Australia. (robert.vincent@adelaide.edu.au)

(Received February 1, 2001; revised May 30, 2001; accepted June 12, 2001.)